Design and Characterization of a Flexible Relative Pressure Sensor With Embedded Micro Pressure Channel Fabricated by Flexible Printed Circuit Board Technology

Yi Chiu, *Member, IEEE*, You-Zen Chen, Chia-Chun Hsieh, and Hao-Chiao Hong, *Senior Member, IEEE*

***Abstract*—This paper presents a relative pressure sensor fabricated by a standard industrial flexible printed circuit board (FPCB) technology. The passive wireless sensor consists of a variable sensing capacitor and a planar coil inductor. When the external pressure is applied to the sensing capacitor, it changes the air gap and shifts the LC resonance frequency which is detected by an antenna wirelessly. The sensing cavity of the variable capacitor is extended to the opening at the end of an embedded pressure channel in the FPCB strip to enable relative pressure measurement. Measurement results showed that the proposed sensor with such an open sensing cavity had much higher frequency sensitivity (up to 0.4 %/mmHg) compared with the sensor with a sealed cavity ($<$ 0.01 %/mmHg in this work and $\leq$ 0.08 in literature). With the enhanced sensitivity, the measured pressure resolution could reach 0.2 mmHg. The potential application of the proposed sensor includes gauge pressure measurement with respect to local atmospheric pressure, such as intracranial pressure (ICP) monitoring, without complicated re-calibration procedures. The flat FPCB structure facilitates applications with limited space for sensor installation, such as in the subdural implantation procedures. Furthermore, the proposed technology enables future development of flexible microfluidic devices.**

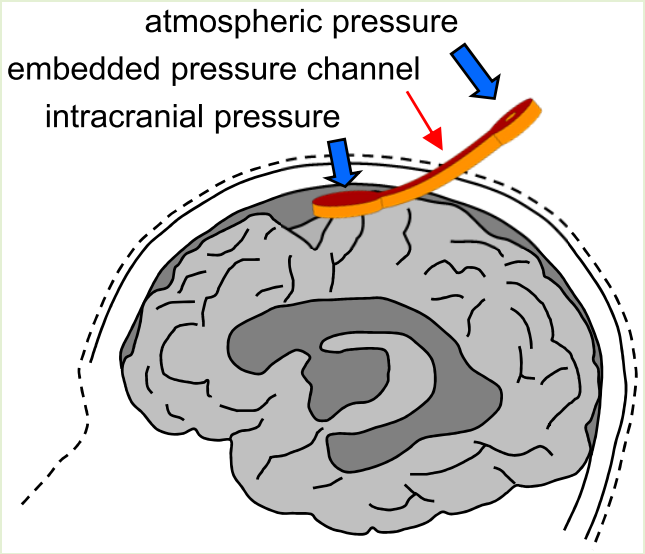

***Index Terms*— Pressure sensor, relative pressure, gauge pressure, intracranial pressure (ICP), wireless, LC resonance, flexible printed circuit board (FPCB), flexible microfluidic devices.**

Manuscript received October 18, 2021; accepted October 25, 2021. Date of publication November 1, 2021; date of current version December 14, 2021. This work was supported in part by the Ministry of Science and Technology, Taiwan, under Grant MOST 104-2221-E-009-156-MY3, Grant 106-2221-E-009-091-MY2, Grant 107-2633-E-009-003, Grant 108-2221-E-009-109, Grant 108-2633-E-009-001, and Grant 109-2639-E-009-001. The associate editor coordinating the review of this article and approving it for publication was Prof. Pai-Yen Chen. *(Corresponding author: Yi Chiu.)*

Yi Chiu and Hao-Chiao Hong are with the Department of Electrical and Computer Engineering, National Yang Ming Chiao Tung University, Hsinchu 300, Taiwan (e-mail: yichiu@mail.nctu.edu.tw; hchong@mail.nctu.edu.tw).

You-Zen Chen was with the Institute of Electrical and Control Engineering, National Yang Ming Chiao Tung University, Hsinchu 300, Taiwan. He is now with Piecemakers Technology, Inc., Hsinchu 300, Taiwan (e-mail: o0912712462@gmail.com).

Chia-Chun Hsieh was with the Institute of Biomedical Engineering, National Yang Ming Chiao Tung University, Hsinchu 300, Taiwan. He is now with AU Optronics Corporation, Hsinchu 300, Taiwan (e-mail: lulu02282003@gmail.com).

Digital Object Identifier 10.1109/JSEN.2021.3124582

I. Introduction

PRESSURE sensors have been widely used in environment/building monitoring, physiological monitoring, industrial control, and automobile sensing. Most micro pressure sensors have sealed pressure sensing cavities for measuring the external pressure with respect to the cavity pressure pre-determined in the fabrication or packaging processes. However, in applications such as the pressure control of cleanroom facilities and negative pressure wards, the pressure difference between two regions is of interest. Furthermore, physiological pressures such as blood pressure (BP), intracranial pressure (ICP) and intraocular pressure (IOP) are defined with respect to the local ambient pressure. Therefore, gauge pressure sensors that measure pressure with respect to local ambience are needed in health and clinical monitoring. These relative pressure measurement sometimes require complicated

sensor packaging and calibration procedures. For example, ICP monitoring is crucial for patients with severe brain injury [1]. ICP sensors need to be calibrated against atmospheric pressure before implantation and in situ re-calibration is desired to account for the barometric pressure variation. Micro pressure sensors have been applied to ICP monitoring because of their high sensitivity and miniaturized sizes [2]–[4]. Nevertheless, in situ re-calibration after sensor insertion or implantation is difficult for the sensors with sealed sensing cavities. In these cases, complex and bulky tubing connection has to be installed. Even though some micro sensors are designed for relative pressure measurement, they typically need extra packaging to connect to different pressure regions and thus making the miniaturization difficult.

In [5], we presented a novel flexible relative pressure sensor manufactured by a standard polyimide (PI) based flexible printed circuit board (FPCB) supplier for applications such as ICP monitoring. The wireless passive LC-resonant sensor has a variable sensing capacitor, an inductor coil and a pressure sensing cavity. A pressure balance channel embedded in the FPCB sensor tail extends the sensing cavity to the external atmospheric environment. Therefore, the relative pressure with respect to the ambient pressure can be readily measured at all time. Such extended-cavity structure also enhances the sensitivity as compared with the sealed-cavity structure seen in most implantable sensors [3], [4], [6]. The flat and flexible sensors can be used in applications such as ICP monitoring where relative pressure measurement is demanded and only minimal and irregular space is available for sensor installation. Furthermore, the proposed design and fabrication technology enables future development of FPCB-based flexible microfluidic devices [7]. In this paper, the details of the sensor design and characterization are presented.

II. Device Principle and Design

Wireless micro passive pressure sensors are typically designed as LC resonators with variable sensing capacitors [3], [4], [8]–[14]. In these capacitive sensors, the applied pressure changes the gap of the sensing capacitors and thus the resonance frequency of the LC-tank resonators, as shown in Fig. 1. The inductors in the LC tank resonators are also used for inductive coupling so that the resonance frequency can be detected by wireless interrogation.

This paper proposes a passive LC-resonant relative pressure sensor fabricated by a standard industrial FPCB technology, as shown in Fig. 2. In the FPCB layout in Fig. 2(a), the planar spiral inductor L and the variable sensing capacitor C_{var} are designed in the sensor head on the left whereas the micro pressure channel is designed in the sensor tail on the right. The proposed sensor is composed of three layers, as shown in Fig. 2(b): the top and the bottom layers are standard FPCB's that contain the coil routing and capacitor electrodes; the middle layer is an acrylic spacer layer that defines the capacitive sensing cavities and pressure channels. The applied external pressure, when acting on the sensing capacitor at the sensor head, changes the capacitor gap and shifts the LC resonance frequency. The sensing cavity of

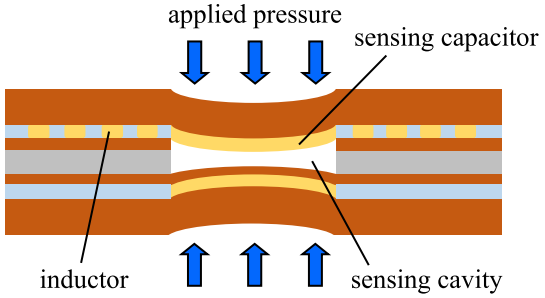

Fig. 1. Principle of traditional wirelsss passive pressure sensor with sealed sensing cavity.

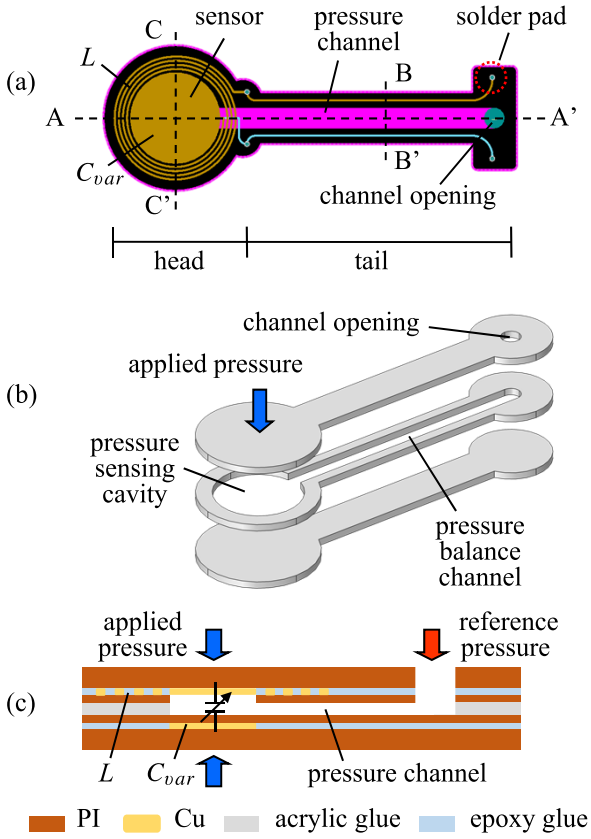

Fig. 2. Structure of proposed sensor with extended cavity, (a) FPCB layout; (b) schematic view before FPCB lamination; (c) AA′ cross-sectional view.

the variable capacitor is extended to the opening at the end of the embedded pressure channel in the flexible sensor tail to enable relative measurement between the applied pressure and the reference pressure, as shown in Fig. 2(c). It is noted that an additional PI layer is laminated on the surface of the bottom capacitor electrode in Fig. 2(c) to prevent the capacitor electrode shortage when the sensor is subjected to large pressure load.

The geometric dimensions and layer thickness of the sensors are summarized in Table I. The thickness of various layers in the FPCB laminates was chosen to minimize the total sensing membrane thickness under the design rules of the manufacturer. According to Table I, the nominal gap g of the sensing capacitor is 53 μ m.

TABLE I
SENSOR GEOMETRIC DIMENSIONS AND LAYER THICKNESS

Parameters	Values
Sensor head diameter	7.0 mm
Sensing cavity diameter	3.2 – 4.4 mm
Sensor tail width	2.4 mm
Pressure channel width	1.5 mm
Top/bottom PI thickness	38 μm
Coverlay PI thickness	13 μm
Copper thickness	12 μm
Epoxy glue thickness	15 μm
Acrylic glue thickness	25 μm

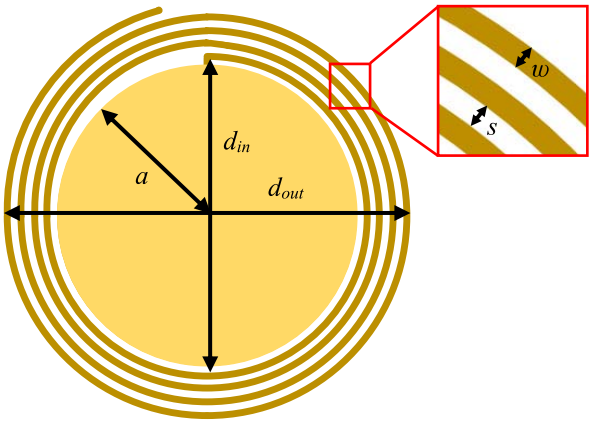

Fig. 3. Design parameters of inductors and capacitors in proposed sensors.

A. Sensor Design: Resonance Frequency

The layout design of the spiral inductor and the sensing capacitor is shown in Fig. 3, where a is the radius of the capacitor electrode, d_{in} and d_{out} are the inner and outer diameters of the spiral, respectively, and w and s are the line width and space of the spiral routing. The resonance frequency of the LC tank in the proposed sensors is

$$f_0 = 1/2\pi\sqrt{LC_{var}}. \tag{1}$$

The inductance L of the spiral inductor can be estimated by [15]

$$L = \frac{\mu_0 n^2 D_{ave} x_1}{2}\left(\ln\frac{x_2}{\rho} + x_3\rho + x_4\rho^2\right), \tag{2}$$

where μ_0 is the permeability of free space, n is the number of turns, D_{ave} is the average spiral diameter

$$D_{ave} = (d_{out} + d_{in})/2, \tag{3}$$

ρ is the fill factor

$$\rho = (d_{out} - d_{in})/(d_{out} + d_{in}), \tag{4}$$

and $x_1 = 1$, $x_2 = 2.46$, $x_3 = 0$ and $x_4 = 0.2$ are constants for circular spirals. The capacitance of the sensing capacitor can be expressed as [16]

$$C_{var} = \epsilon_0\frac{\pi a^2}{g} + 2\epsilon_0 a\ln\frac{32a}{eg}, \tag{5}$$

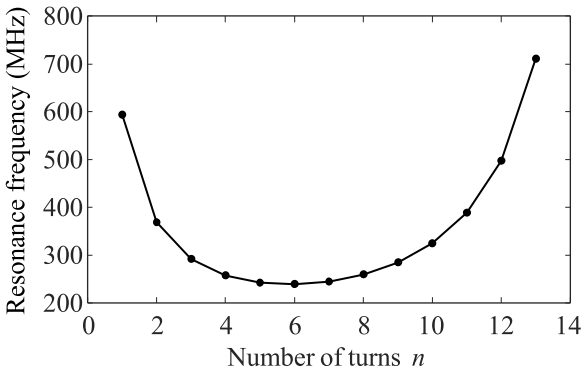

Fig. 4. Calculated resonance frequency for fixed outer diameter $d_{out} = 6$ mm.

where ϵ_0 is the permittivity of free space, a is the radius of the circular electrodes, g is the capacitor gap, and e is the Euler's number. The two terms in Eq. 5 account for the parallel-plate capacitance and the fringing capacitance, respectively.

For the proposed sensors with fixed areas, increasing the number of coil turns will increase its inductance while decreasing the capacitor area and its capacitance. In Fig. 4, the resonance frequency calculated from Eqs. 1, 2 and 5 is plot as a function of the number of turns n for a coil with an outer diameter $d_{out} = 6$ mm and minimum line width w and space s of 100 μm. It can be seen that the resonance frequency remains almost constant and insensitive to the sensor design for n between 4 and 8. In this study, four sensors with $d_{out} = 6$ mm and $n = 4, 5, 6, 7$ are designed and tested.

B. Sensor Design: Sensitivity

When a net pressure P_{net} acts upon a circular membrane of radius a, the central deflection is

$$w_0 = P_{net}a^4/64D, \tag{6}$$

where $D = Et^3/12(1-\nu^2)$ is the flexural rigidity of the membrane and E, t, and ν are the Young's modulus, thickness, and Poisson's ratio of the membrane, respectively. The proposed passive LC resonant pressure sensors in this study have two circular flexible sensing membranes as shown in Fig. 2. The central deflections are

$$w_{0i} = P_{net}a^4/64D_i, \tag{7}$$

where $i = 1$ or 2 for the two membranes. The capacitance between the sensing membranes is [6],

$$C_{var} = C_0\sqrt{\frac{g}{w_{0t}}}\tanh^{-1}\sqrt{\frac{w_{0t}}{g}}, \tag{8}$$

where g is the initial sensing gap, $C_0 = \epsilon_0\pi a^2/g$ is the parallel-plate capacitance without deformation, and

$$w_{0t} = w_{01} + w_{02} = P_{net}a^4/64D_t \tag{9}$$

is the sum of the central deflections of the two membranes and $D_t^{-1} = D_1^{-1} + D_2^{-1}$.

The sensitivity S of the proposed sensor is defined as the resonance frequency shift per unit pressure,

$$S = \frac{df_0}{dP}(\text{MHz/mmHg}). \tag{10}$$

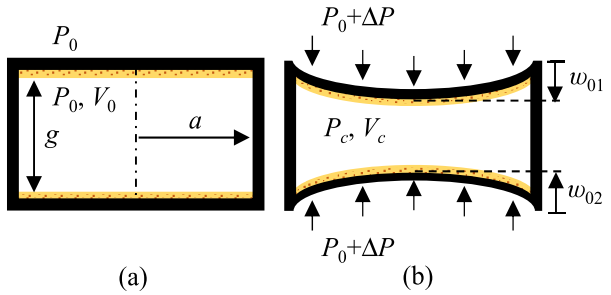

Fig. 5. Trapped air effect in sealed pressure sensor; (a) initial and (b) compressed states.

Alternatively, a relative sensitivity S_r can be defined,

$$S_r = \frac{1}{f_0}\frac{df_0}{dP}(\%\ /\text{mmHg}). \tag{11}$$

For small deflection, Eq. 8 can be approximated as

$$C \approx C_0\left(1+\frac{1}{3}\frac{w_{0t}}{g}\right). \tag{12}$$

Therefore, the capacitance sensitivity with respect to pressure is

$$\frac{dC}{dP_{net}} = \frac{C_0}{3g}\frac{a^4}{64D_t}, \tag{13}$$

and the relative frequency sensitivity defined in Eq. 11 is

$$S_r = -\frac{1}{2C_0}\frac{dC}{dP_{net}} = -\frac{a^4}{384gD_t}. \tag{14}$$

The sensitivity of pressure sensors depends on whether the sensing cavity is sealed or extended to the atmosphere such as in the proposed sensor in Fig. 2. For sensors with sealed cavities, the internal pressure of the trapped air in the cavities is increased when the sensing membranes are depressed by the external pressure. Thus the net pressure across the membranes is reduced, resulting in reduced sensitivity. Fig. 5 shows the cross section of a sealed-cavity pressure sensor before and after the pressure ΔP is applied. For an isothermal process, the volume V and pressure P of the cavity are related by

$$P_0V_0 = P_cV_c, \tag{15}$$

where the subscripts 0 and c refer to the initial and compressed states, respectively, as shown in Fig. 5. For circular sensing membranes, the trapped air effect can be expressed as [6]

$$P_0V_0 = P_cV_0\left(1-\frac{w_{0t}}{3g}\right). \tag{16}$$

For small deflection, Eq. 16 can be approximated as

$$P_c = P_0\left(1-\frac{w_{0t}}{3g}\right)^{-1} \approx P_0\left(1+\frac{w_{0t}}{3g}\right). \tag{17}$$

For the applied pressure ΔP with respect to a reference pressure P_0 as shown in Fig. 5, the net pressure P_{net} across the membranes obtained from Eqs. 9 and 17 is,

$$\begin{aligned} P_{net} &= (P_0+\Delta P) - P_c \\ &= \Delta P - \frac{w_{0t}}{3g}P_0 = \Delta P - \frac{P_0a^4}{192gD_t}P_{net}, \end{aligned} \tag{18}$$

TABLE II
FLEXURAL RIGIDITY OF SENSING MEMBRANES

	Parameters	Top	Bottom
PI	Young's modulus (E)	2.5 GPa	
	Poisson's ratio (ν)	0.34	
	Thickness (t)	38 μm	66 μm
Cu	Young's modulus (E)	128 GPa	
	Poisson's ratio (ν)	0.36	
	Thickness (t)	12 μm	
D_i	Flexural rigidity	7.6×10^{-5} Pa·m^3	3.2×10^{-4} Pa·m^3
D_t	Flexural rigidity	6.2×10^{-5} Pa·m^3	

Thus,

$$P_{net} = \Delta P\left(1+\frac{P_0a^4}{192gD_t}\right)^{-1} = \frac{\Delta P}{1+k_{ta}}, \tag{19}$$

where the factor

$$k_{ta} = P_0a^4/192gD_t \tag{20}$$

represents the effect of trapped air. The relative sensitivity in Eq. 14 can be rewritten as,

$$S_r = -\frac{1}{2C_0}\frac{dC}{d\Delta P} = -\frac{a^4}{384gD_t(1+k_{ta})}. \tag{21}$$

It is noted that for sensors with extended cavities as shown in Fig. 2, the trapped air factor k_{ta} is zero by taking P_0 to zero or g to infinity in Eq. 20.

The material properties, geometric parameters, and calculated flexural rigidities of the composite top and bottom sensing membranes are listed in Table II. For the proposed sensors in this paper, the cavity gap g is 53 μm and the typical membrane radius a is 2 mm. Therefore for $P_0 = 1$ atm, the trapped air factor k_{ta} is about 2.6 for sensors with sealed cavities.

In this paper, two types of sensors were designed for comparison. Sensors with pressure balance channels are R-sensors for relative pressure measurement; sensors with sealed cavities and no pressure channels are A-sensors for absolute pressure measurement. For the above typical design, therefore, the sensitivity of the R-sensors with open cavities will be enhanced by a factor of $1 + k_{ta} = 3.6$ with respect to the A-sensors with sealed cavities. The sensitivities of the R-sensors were simulated by using the finite-element-method (FEM) simulation tool Coventorware. Table III summarizes the theoretical and simulated sensitivities of various sensor designs.

III. SENSOR FABRICATION

The proposed sensors were manufactured by a local PCB manufacturer by using a standard 4-layer polyimide-based FPCB process. Adhesiveless flexible copper clad laminates (FCCL) were used for the top and bottom FPCB's to reduce the overall thickness of the sensors. The manufacturing process is shown in Fig. 6. The coils and electrodes are first patterned in the top and bottom FPCB's. Coverlay PI films are then laminated on the FPCB's for protection and insulation (Figs. 6(a) and (b)). It is noted that the coverlay PI for the top FPCB is laser-cut in the sensor and channel areas to reduce the sensing membrane thickness before lamination (Fig. 6(a)).

TABLE III
THEORETICAL AND SIMULATED SENSITIVITY

Number of coil turns	Sensor type	k_{ta}	Sensitivity S_r (%/mmHg)	
			Theoretical	Simulated
4	A	3.8	0.052	-
	R	0	0.25	0.22
5	A	2.6	0.047	-
	R	0	0.17	0.15
6	A	1.7	0.041	-
	R	0	0.11	0.10
7	A	1.1	0.034	-
	R	0	0.07	0.06

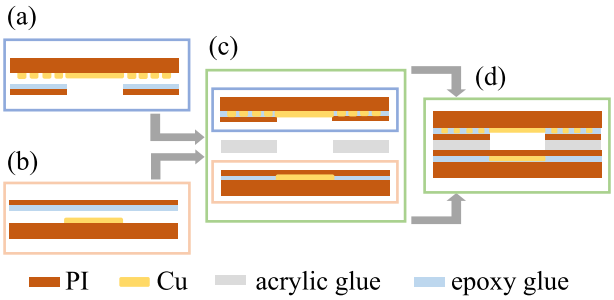

Fig. 6. FPCB manufacturing process of proposed sensor. (a) Top FPCB before lamination, (b) bottom FPCB before lamination, (c) top FPCB, spacer layer, and bottom FPCB before lamination, (d) laminated device.

In Fig. 6(c), a sheet of acrylic adhesive is laser-cut to define the sensing cavity and pressure channel. The acrylic layer also serves as a spacer layer to define the sensing cavity and its gap. The top/bottom FPCB's and the acrylic layer are then laminated to form the final device (Fig. 6(d)).

All the lamination processes were conducted at 180 °C for 700 seconds under 700 kg/cm^2 pressure. After the pressurized process, the laminates were kept at 180 °C for another hour to fully cure the adhesive and release internal stress. The symmetric stacking design of the top and bottom FPCB's also helped reduce the stress-induced deformation after the laminates were cooled to room temperature.

Fig. 7 shows the photographs of the manufactured FPCB sensors of various designs. The devices with opening at the end of the pressure channels are R-sensors (Fig. 7(b), (c)); the devices without opening are A-sensors (Fig. 7(d), (e)). The elevated temperature and pressure during lamination caused reflow of the acrylic spacer layer. To investigate the effect of reflow on the yield of fabrication, pressure channels with different widths were designed and tested. Fig. 8 shows the BB' cross sections of the pressure channels with different channel widths. It can be seen the reflow resulted in the obstruction of channels for small channel width (Fig. 8(a)). Therefore, a channel width of 1.5 mm (Fig. 8(b)) was adopted in the following testing and discussion to avoid this problem.

IV. MEASUREMENT AND DISCUSSION

The sensors were designed with solder pads in the FPCB, as shown in Fig. 2(a), so that both wired and wireless tests can be preformed. The fabricated sensors were first tested with

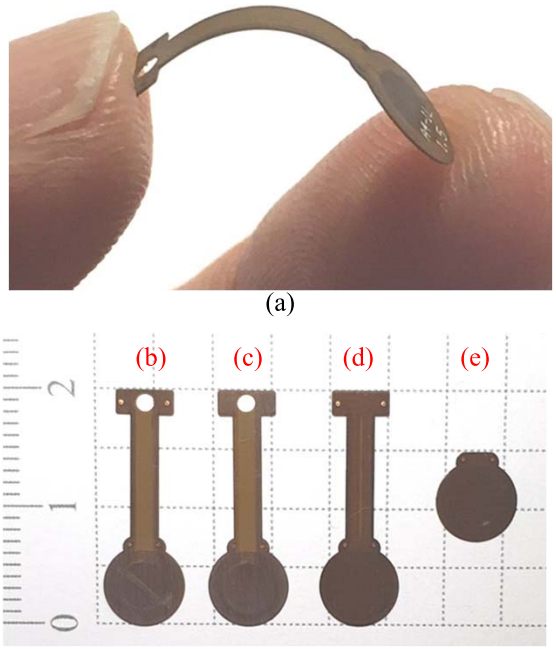

Fig. 7. (a) Fabricated FPCB flexible pressure sensor; (b) and (c): relative sensors (R-sensors); (d) and (e): absolute sensors (A-sensors).

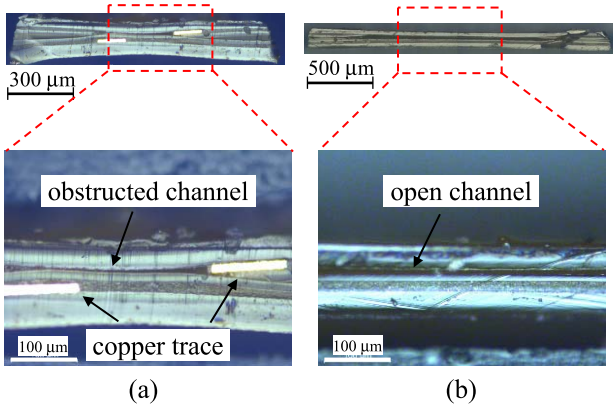

Fig. 8. Cross sections of pressure balance channels with (a) 0.25 mm channel width; and (b) 1.5 mm channel width.

soldered wires via a vector network analyzer (VNA) (Keysight E5071B) to check their resonance frequency. It was found that the resonance frequencies of the A-sensors and R-sensors were about 50% and 70% of the design values, respectively. Since the resonance frequency is determined by the gap of the sensing capacitor, the overall reduction of resonance frequency is attributed to the softening, reflow, and thinning of the spacer and adhesive layers, as can be seen in Fig. 8, during the lamination processes. The reduced sensing gap increases the capacitance and thus reduces the resonance frequency.

The surface topology of fabricated sensor heads was measured by a line scan along CC' in Fig. 2(a) with a digital microscope (Keyence VHX 6000), as shown in Fig. 9. The center depression of A-sensors shown in Fig. 9(a) is caused by the pressure imbalance between the sealed sensing cavity and the ambient atmosphere after cooling down to room

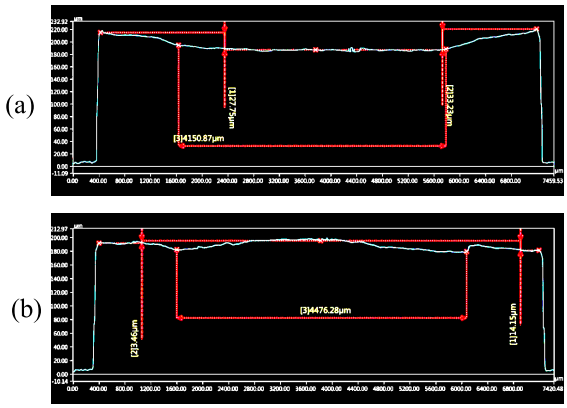

Fig. 9. Surface topology of (a) A-sensor; and (b) R-sensor. The depression in the center of the A-sensor results in lower resonance frequency.

temperature from the elevated temperature in the lamination processes. In contrast, the R-sensors have relatively flat surface (Fig. 9(b)) because the pressure in the sensing cavity and the ambience is always balanced by the pressure channels. The depressed sensing capacitors in the A-sensors results in their lower resonance frequency compared with the R-sensors.

A home-built acrylic pressure chamber, as shown in Fig. 10(a), was used for sensor characterization. The feedthrough and pressure ports allow signal wires and sensor tails to go through the chamber, respectively, while maintaining the internal chamber pressure. The chamber can be filled with air or water during test to emulate different application scenarios and check the sensors' water-tightness. The chamber pressure was monitored with a commercial pressure sensor that can operate both in air or liquid. Various testing conditions are discussed in the following sections.

A. Functional Test

To verify that the pressure balance channels in R-sensors were not obstructed by spacer reflow and the sensing cavities in A-sensors were properly sealed in the lamination steps, wired sensors of both types were placed in the pressure chamber and tested with the network analyzer, as shown in Fig. 10(b). The measured resonance frequency variation vs. the applied pressure is shown in Fig. 11. The R-sensor did not show frequency variation when the chamber pressure was changed, implying an unobstructed pressure channel that balanced the pressure across the sensing membranes. On the other hand, the resonance frequency of the A-sensor varied with the chamber pressure, indicating the sensing cavity was successfully sealed in the lamination process.

B. Wired Pressure Test

Pressure tests of wired sensors were conducted in the setup shown in Fig. 10(c). The sensor heads were kept inside the chamber while the sensor tails were exposed to the ambience through the pressure port. It is noted that both R-sensors (Fig. 7(b)) and A-sensors (Fig. 7(d)) were tested in the same manner as shown in Fig. 10(c) even though an R-sensor is shown in the figure as an example. In the case of an R-sensor,

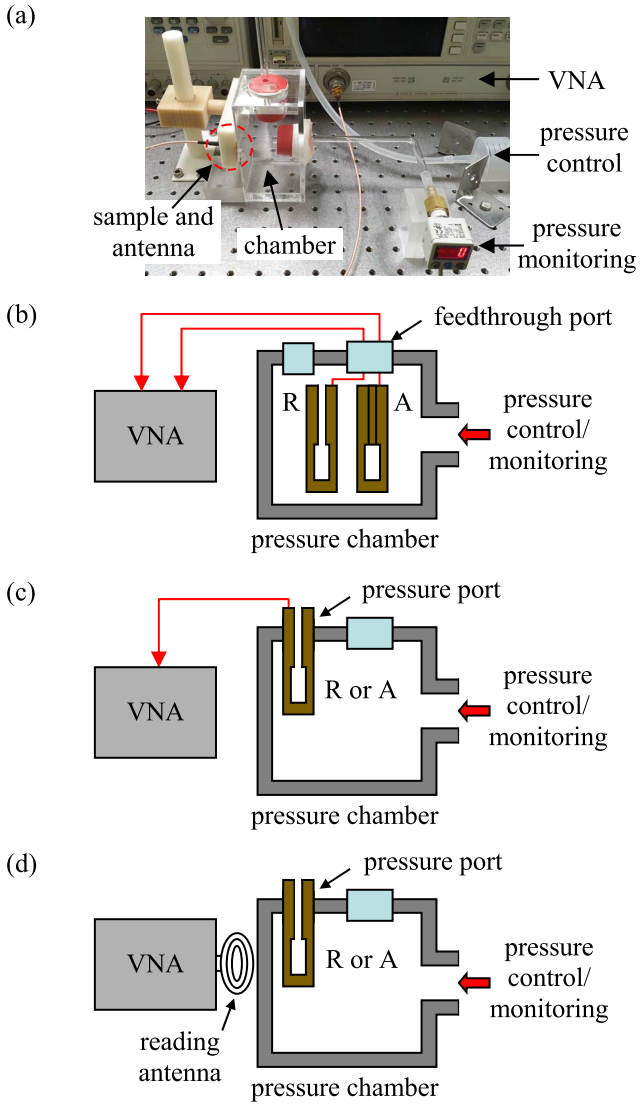

Fig. 10. Sensor characterization setup, (a) actual setup; (b) wired functional test; (c), wired pressure test; and (d) wireless pressure test.

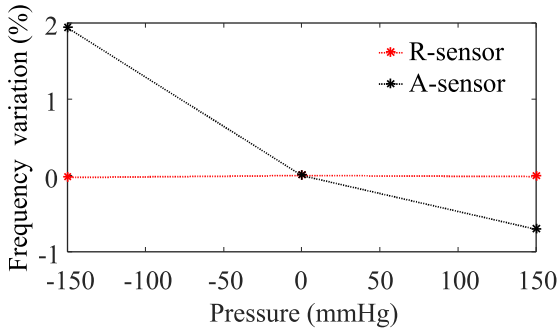

Fig. 11. Measured frequency variation in functional test. The pressure in the horizontal axis is expressed with respect to the atmospheric pressure.

the pressure channel in the sensor tail connected the sensing cavity to the ambient pressure. The sensors were tested with the chamber filled with air or water. The resonance frequency was found from the VNA impedance measurement at which the imaginary part was zero.

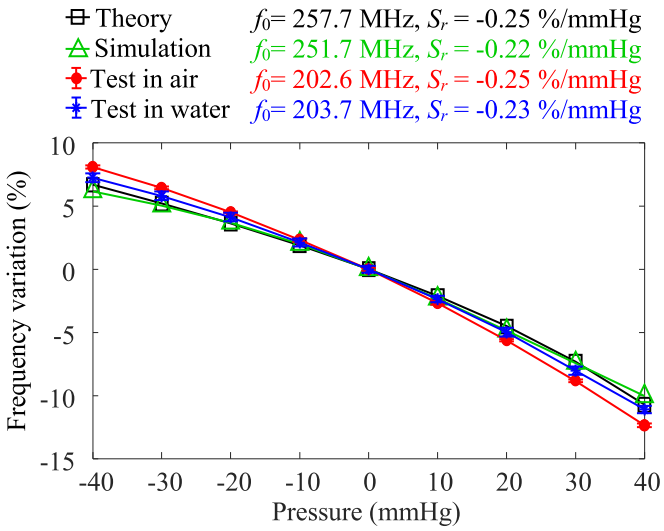

Fig. 12. Resonance frequency variation and sensitivity of a wired 4-turn R-sensor.

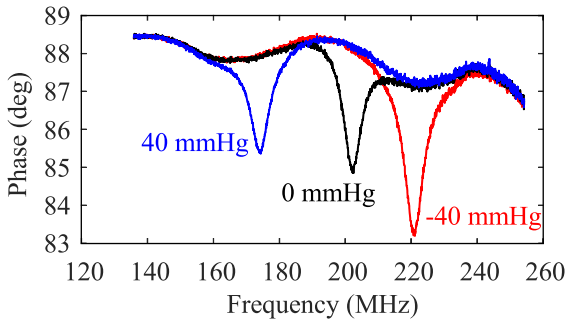

Fig. 13. Phase dip measurement of a typical sensor.

Fig. 12 shows the resonance frequency variation and sensitivity S_r of a typical R-sensor in the wired test setup. The sensor performance is consistent in different media (air or water) and agrees well with theoretical modeling and simulation. The small discrepancy can be attributed to the sensor's dimensional errors due to fabrication tolerance. The characteristics of wired sensors of various designs are summarized in Table IV and discussed in the following sections.

C. Wireless Pressure Test

The wireless sensor test setup is shown in Fig. 10(d). The flat FPCB sensor was placed on the wall inside the chamber and characterized by the VNA using inductive coupling from outside. The thickness of the chamber wall, and thus the distance between the sensor and the reading antenna, was 3 mm. The resonance frequency was determined from the phase dip of measured impedance, such as shown in Fig. 13.

Fig. 14 shows the resonance frequency variation and sensitivity S_r of a typical R-sensor in the wireless test setup. Sensor performance and general trend similar to Fig. 12 for wired measurement can be observed. The characteristics of wireless sensors of various designs are summarized in Table IV.

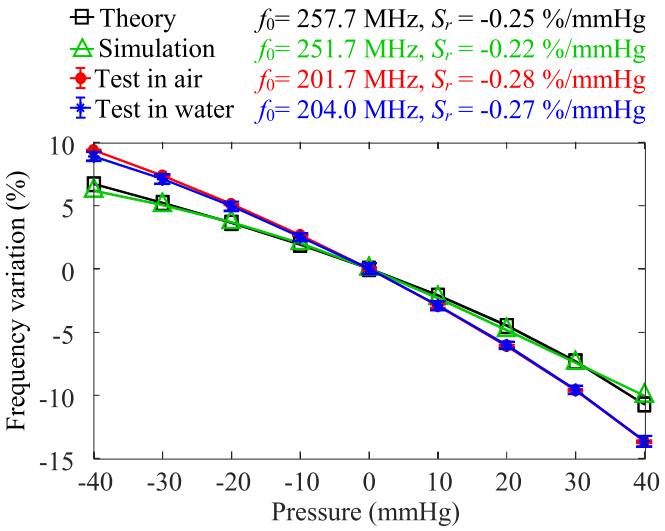

Fig. 14. Resonance frequency variation and sensitivity of a wireless 4-turn R-sensor.

TABLE IV
SENSOR TEST SUMMARY

1	# coil turns				4		5		6		7	
2	Test medium				Air	Water	Air	Water	Air	Water	Air	Water
3	f_0[1]	T[4]			257.7		242.3		239.4		245.1	
4		M[5]	A	WD[6]	117.6	115.5	112.4	104.7	110.6	103.0	112.9	108.7
5				WL[7]	122.4	119.2	115.2	110.5	113.0	106.9	115.3	107.8
6			R	WD	202.6	203.7	145.2	140.6	152.6	149.7	170.3	159.6
7				WL	201.7	204.0	146.0	150.2	155.3	156.5	176.3	175.4
8	S_r[2]	T	A		0.04		0.04		0.03		0.03	
9		M		WD	0.004	0.004	0.008	0.008	0.003	0.003	0.006	0.006
10				WL	0.005	0.006	0.003	0.004	0.004	0.005	0.007	0.005
11		T	R		0.25		0.17		0.11		0.07	
12		M		WD	0.25	0.23	0.39	0.32	0.20	0.18	0.11	0.09
13				WL	0.28	0.27	0.40	0.37	0.20	0.18	0.11	0.10
14	σ_P[3]	M	A	WD	0.78	0.66	0.29	0.37	0.56	2.5	0.29	0.65
15				WL	1.1	0.52	1.2	1.6	0.55	0.60	0.46	0.86
16			R	WD	0.35	0.55	0.29	0.41	0.31	0.69	0.18	0.25
17				WL	0.28	0.66	0.16	0.35	0.20	0.35	0.34	0.53

[1] Resonance frequency at 0 mmHg (MHz) [2] Sensitivity at 0 mmHg (%/mmHg)
[3] Pressure resolution at 0 mmHg (mmHg)
[4] Theoretical value [5] Measured value [6] Wired test [7] Wireless test

D. Discussion

Table IV summarizes the sensor characteristics of various designs under various test conditions. A number of general trends can be observed.

1. The measured resonance frequency f_0 of both A-sensors and R-sensors are lower than the theoretical values, as shown in rows 3-7, due to the reduced capacitor gap caused by the lamination processes at elevated temperature and pressure. The R-sensors (rows 6-7) have higher resonance frequency than the A-sensors (rows 4-5), as explained in the beginning of Sec. IV. This indicates that the sensing membranes of the A-sensors have larger initial depression and smaller capacitor gaps than the R-sensors.

TABLE V
PERFORMANCE COMPARISON OF WIRELESS PASSIVE CAPACITIVE PRESSURE SENSORS

	[3]	[4]	[10]	[12]	[13]	[14]	This work	
Type	A	A	A	A	A	A	A	R
Test range (mmHg)	0 ~ 70	0 ~ 100	0 ~ 50	0 ~ 230	0 ~ 200	0 ~ 250	-40 ~ 40	
f_0 (MHz)	31.2	2777	63.7	183	792	262.25	113.0	155.3
S_r (%/mmHg)	0.027	0.081	0.022	0.052	0.036	0.036	0.004	0.20
Resolution (mmHg)	2.5	-	~ 1	-	-	-	0.55	0.20

2. The resonance frequency and sensitivity obtained from the wired (WD) and the wireless (WL) measurements agree with each other well.
3. The resonance frequency and sensitivity obtained from measurement in air and in water also agree with each other well, indicating the fringing capacitance, which is affected by the surrounding medium more significantly, does not play a major role compared with the parallel-plate sensing capacitance. However, the small difference may still cause concerns in critical measurements such as ICP monitoring. In such applications, therefore, it is necessary to calibrate the sensor and find its resonance frequency and sensitivity at atmospheric pressure (0 mmHg) before insertion. This calibration process is preferably carried out in a medium that can emulate body fluid or cerebral conditions to alleviate the effect of measurement conditions on the resonance frequency.
4. The measured sensitivity S_r of the R-sensors (rows 12-13) is slightly higher than the theoretical values (row 11) while that of the A-sensors (rows 9-10) is much lower than the corresponding theoretical value (row 8). The reason of the higher sensitivity of the R-sensors can be attributed to the reduced capacitor gap, as shown in Eq. 14. On the other hand, the reasons for the reduced sensitivity of the A-sensors are not known yet. It is possible that the initial larger depression of the A-sensors results in high internal stress in the sensing membranes, increases its rigidity, and lowers its sensitivity. Further investigations are needed to clarify this issue.

The measured performance of a wireless 6-turn FPCB sensor is summarized in Table V and compared to literature. The proposed R-sensor has higher sensitivity than the A-sensors in the present work and the literature. Due to the high sensitivity, the proposed R-sensors can achieve a resolution as low as 0.2 mmHg.

V. CONCLUSION

A wireless relative pressure sensor was demonstrated by using a standard commercial FPCB service. The flat and flexible sensors can be used in applications such as ICP monitoring where the available space for sensor installation is limited. The pressure balance channel embedded in the FPCB enables direct measurement of ICP with respect to the local atmospheric pressure without complicated re-calibration procedures. The open-cavity structure of the proposed sensors alleviates the trapped air effect in traditional sealed-cavity design, increases its sensitivity up to 0.4 %/mmHg, and improves the pressure sensing resolution to as low as 0.2 mmHg. Furthermore, the proposed FPCB device design enables future development of flexible microfluidic devices.

ACKNOWLEDGMENT

The authors acknowledge the support of the National Center for High-performance Computing, the Taiwan Semiconductor Research Institute, and the National Yang Ming Chiao Tung University Nano Facility Center, Taiwan, R.O.C., for various simulation, fabrication, and characterization tools.

REFERENCES

[1] A. Ristic, R. Sutter, and L. A. Steiner, "Current neuromonitoring techniques in critical care," *J. Neuroanaesthesiol. Crit. Care*, vol. 2, no. 2, pp. 97–103, 2015.
[2] X. Meng, K. D. Browne, S.-M. Huang, D. K. Cullen, M.-R. Tofighi, and A. Rosen, "Dynamic evaluation of a digital wireless intracranial pressure sensor for the assessment of traumatic brain injury in a swine model," *IEEE Trans. Microw. Theory Techn.*, vol. 61, no. 1, pp. 316–325, Jan. 2013.
[3] M. H. Behfar, T. Björninen, E. Moradi, L. Sydänheimo, and L. Ukkonen, "Biotelemetric wireless intracranial pressure monitoring: An *in vitro* study," *Int. J. Antennas Propag.*, vol. 2015, Nov. 2015, Art. no. 918698.
[4] L. Y. Chen *et al.*, "Continuous wireless pressure monitoring and mapping with ultra-small passive sensors for health monitoring and critical care," *Nature Commun.*, vol. 5, no. 1, pp. 1–10 2014.
[5] Y. Chiu, Y.-Z. Chen, C.-C. Hsieh, and H.-C. Hong, "A wireless gauge pressure sensor with enhanced sensitivity fabricated by flexible PCB technology for intracranial pressure sensing," in *Proc. IEEE SENSORS*, Oct. 2019, pp. 1–4.
[6] H. Y. Lee and B. Choi, "Theoretical and experimental investigation of the trapped air effect on air-sealed capacitive pressure sensor," *Sens. Actuators A, Phys.*, vol. 221, pp. 104–114, Jan. 2015.
[7] D. Moschou and T. Angeliki, "The lab-on-PCB approach: Tackling the μTAS commercial upscaling bottleneck," *Lab Chip*, vol. 17, no. 8, pp. 1388–1405, 2017.
[8] P.-J. Chen, S. Saati, R. Varma, M. S. Humayun, and Y.-C. Tai, "Wireless intraocular pressure sensing using microfabricated minimally invasive flexible-coiled LC sensor implant," *J. Microelectromech. Syst.*, vol. 19, no. 4, pp. 721–734, Aug. 2010.
[9] N. Xue, S.-P. Chang, and J.-B. Lee, "A SU-8-based microfabricated implantable inductively coupled passive RF wireless intraocular pressure sensor," *J. Microelectromech. Syst.*, vol. 21, no. 6, pp. 1338–1346, Dec. 2012.
[10] G. Chitnis, T. Maleki, B. Samuels, L. B. Cantor, and B. Ziaie, "A minimally invasive implantable wireless pressure sensor for continuous IOP monitoring," *IEEE Trans. Biomed. Eng.*, vol. 60, no. 1, pp. 250–256, Jan. 2013.
[11] Q. Tan *et al.*, "A LC wireless passive temperature-pressure-humidity (TPH) sensor integrated on LTCC ceramic for harsh monitoring," *Sens. Actuators B, Chem.*, vol. 270, pp. 433–442, Oct. 2018.
[12] J. Park, J.-K. Kim, S. J. Patil, J.-K. Park, S. Park, and D.-W. Lee, "A wireless pressure sensor integrated with a biodegradable polymer stent for biomedical applications," *Sensors*, vol. 16, no. 6, p. 809, 2016.
[13] W.-J. Deng, L.-F. Wang, L. Dong, and Q.-A. Huang, "LC wireless sensitive pressure sensors with microstructured PDMS dielectric layers for wound monitoring," *IEEE Sensors J.*, vol. 18, no. 12, pp. 4886–4892, Jun. 2018.
[14] S.-H. Lo, M.-X. Xu, and Y.-J. Yang, "A wireless parylene-based cardiovascular pressure sensor with mxene film," in *Proc. 20th Int. Conf. Solid-State Sens., Actuators Microsyst. Eurosensors*, Jun. 2019, pp. 2231–2234.
[15] S. S. Mohan, M. D. M. Hershenson, S. P. Boyd, and T. H. Lee, "Simple accurate expressions for planar spiral inductances," *IEEE J. Solid-State Circuits*, vol. 34, no. 10, pp. 1419–1424, Oct. 1999.
[16] G. J. Sloggett, N. G. Barton, and S. J. Spencer, "Fringing fields in disc capacitors," *J. Phys. A, Math. Gen.*, vol. 19, no. 14, p. 2725, 1986.

Yi Chiu (Member, IEEE) received the B.S. degree in electrical engineering from the National Taiwan University, Taiwan, in 1988, and the M.S. and Ph.D. degrees in electrical and computer engineering from Carnegie Mellon University, Pittsburgh, PA, USA, in 1991 and 1996, respectively.

Dr. Chiu is currently a Professor with the Department of Electrical and Computer Engineering, National Yang Ming Chiao Tung University, Taiwan. His research interests include electrostatic and electromagnetic energy harvesting, micro sensors, CMOS-MEMS sensors, PCB MEMS, and optical MEMS. He has served as a member for the Technical Program Committee in IEEE Optical MEMS and Nanophotonics, Asia–Pacific Conference of Transducers and Micro-Nano Technology (APCOT), IEEE SENSORS, and International Conference on Solid-State Sensors, Actuators and Microsystems (Transducers).

You-Zen Chen, photograph and biography not available at the time of publication.

Chia-Chun Hsieh, photograph and biography not available at the time of publication.

Hao-Chiao Hong (Senior Member, IEEE) received the B.S., M.S., and Ph.D. degrees in electrical engineering from the National Tsing Hua University, Hsinchu, Taiwan, in 1990, 1992, and 2003, respectively. From 1997 to 2001, he was with Taiwan Semiconductor Manufacturing Company (TSMC), where he developed mixed-signal IPs for customers and process vehicles. He joined Intellectual Property Library Company, Hsinchu, as the Senior Manager with the Analog IP Department in August 2001. He has been with the National Yang Ming Chiao Tung University (NYCU), Hsinchu, since February 2004, where he is currently a Full Professor with the Institute of Electrical and Computer Engineering. He holds nine U.S. patents, ten Taiwan patents, and four China patents. His main research interests include the sensor interface circuit design, design-for-testability, built-in self-test, and calibration techniques for mixed-signal circuits, high performance mixed-signal IC, and neural network accelerator designs. Dr. Hong received the best paper awards from the 2009 International Symposium on VLSI Design, Automation, and Test (VLSI-DAT), the tenth VLSI Test Technology Workshop (VTTW), and the third IEEE International Conference on Applied System Innovation (ICASI). He also received the Best Advisor Award in the IC design competition of the twelfth Macronix Golden Silicon Award in 2012.